DOI: 10.19884/j.1672-5220.202402004

Cellulose-Based Nanofibers Electrospun from Cuprammonium Solutions: Preparation, Mechanical and Antibacterial Properties

DANISH Iqbal[1,2,3], ZHAO Renhai[1,2], MUHAMMAD Ilyas Sarwar[3], NING Xin[1,2*]
1. Industrial Research Institute of Nonwovens & Technical Textiles, College of Textiles & Clothing, Qingdao University, Qingdao 266071, China
2. Shandong Engineering Research Center for Specialty Nonwoven Materials, Qingdao University, Qingdao 266071, China
3. Fiber Technology Section, Central Cotton Research Institute, Multan 60000, Pakistan

Abstract: Nanofibers based on cellulose are highly desired due to their remarkable biocompatibility and attractive physical and biochemical characteristics. The current research describes a simple electrospinning process and the nano-materials therefrom, utilizing the classical cellulose-cuprammonium solution without the more exotic chemical solvent combinations. Furthermore, without the use of organic solvents, a binary polymer system with the addition of polyethylene oxide (PEO) is introduced to improve the robustness of the electrospinning and the properties of the final material. The impacts of the cellulose source, cellulose mass fraction and PEO formulation on spinnability, fiber morphology and mechanical properties are investigated. Nanofibers with diameters ranging from 130 nm to 382 nm are successfully fabricated. The presence of copper in the fabricated material is confirmed by using the X-ray photoelectron spectroscopy (XPS) analysis. The cuprammonium process significantly changes the original crystalline structure of cellulose I into cellulose Ⅲ within the nanofiber morphology. The nanofibrous membranes also demonstrate notable antibacterial characteristics for *Staphylococcus aureus* (*S. aureus*) and *Escherichia coli* (*E. coli*).

Key words: cellulose; electrospinning; cuprammonium solution; polyethylene oxide (PEO); antibacterial activity
CLC number: TS102 **Document code**: A
Article ID: 1672-5220(2024)06-0582-13

Open Science Identity (OSID)

0 Introduction

As the most abundant organic polymer on earth, cellulose is a vital component of plant cell walls, providing structural support and contributing to plant function. Moreover, due to its renewable nature and biodegradability, cellulose has been extensively studied and utilized in various industrial applications[1]. The research on nanofiber generation based on cellulose has attracted considerable interest in the scientific community due to its distinctive characteristics and wide-ranging application possibilities in protective clothing, biomedical areas, filtration and separation[2-4]. Plants are considered as the primary source of cellulose, and cellulose may also be derived from several other sources, like animals, fungi and algae[5]. Recent advancements in nanotechnology have paved the way for the development of cellulose-based nanofibers. These nanofibers, derived from natural cellulose, exhibit remarkable properties such as high mechanical strength, chemical modifiability, and a high surface area. Furthermore, they are biodegradable, aligning with the global trend towards sustainable and environmentally friendly materials[6].

Cellulose, however, lacks solubility in most organic solvents. This is attributed to the substantial presence of inter- and intra-molecular hydrogen bonds linked to hydroxyl groups in the glycosidic rings, rendering cellulose a highly robust and stiff polymer. This characteristic necessitates precise solvent blends that can effectively weaken hydrogen bonding, thereby inducing the separation of cellulose molecules[7]. Solvents applied for the dissolution of cellulose are classified into two groups: derivatizing solvents and non-derivatizing solvents. Cellulose is subject to a chemical covalent modification process when it is dissolved in derivatizing solvents, substituting some hydroxyl groups with ester, ether or acetal groups. This modification chemically transforms cellulose into soluble cellulose derivatives. These cellulose derivatives include cellulose acetate, cellulose nitrate, cellulose xanthate, cellulose carbamate and cellulose phosphate[8-9].

The non-derivatizing solvents rely on a physical alteration of intermolecular interactions instead of a

Received date: 2024-02-15
Foundation items: Key Project of State Key Laboratory of Bio-Fibers and Eco-Textiles of Qingdao University, China (No. RZ2000003348); High Level Talents Research Start-Up Fund, China (No. DC1900000746); China Postdoctoral Science Foundation (No. 2024M751568); Shandong Province Postdoctoral Innovation Project, China (No. SDCX-ZG-202400294)
* Correspondence should be addressed to NING Xin, email: xning@qdu.edu.cn
Citation: DANISH I, ZHAO R H, MUHAMMAD I S, et al. Cellulose-based nanofibers electrospun from cuprammonium solutions: preparation, mechanical and antibacterial properties[J]. *Journal of Donghua University (English Edition)*, 2024, 41(6): 582-594.

chemical modification. Illustrations of such instances comprise metal-cellulose complexes encompassing a transition metal and an ammonium or amine constituent[10]. Various non-derivatizing techniques are available, including the utilization of aqueous alkalies such as cuprammonium hydroxide, polyethylene glycol, thiourea, lithium hydroxide with urea, sodium hydroxide complexes with urea, concentrated molten inorganic salt hydrates and dimethylacetamide/lithium chloride, *n*-methylmorpholine *n*-oxide dimethyl and sulfoxide/tetra-*n*-butylammonium fluoride[11].

The cuprammonium system is a non-derivatizing solvent that facilitates the dissolution of cellulose by intermolecular interactions without altering the cellulose chains, hence enabling cellulose solubilization. The cuprammonium ion always pairs up with the hydroxyl groups at positions C_2 and C_3 of the glucopyranose units in the cellulose structure[12] (Fig. 1). This interaction reduced intermolecular hydrogen bonding within cellulose[13], thereby facilitating the separation of cellulose molecules. The dissolution mechanism has been thoroughly examined and confirmed by various researchers[14-15]. Copper was predominantly present in the amorphous region, leading to a reorganization of the molecular arrangement of cellulose[16]. During the cellulose recovery process, the copper hydroxide lay on the surface of the fabric while the ammonia component evaporated[17].

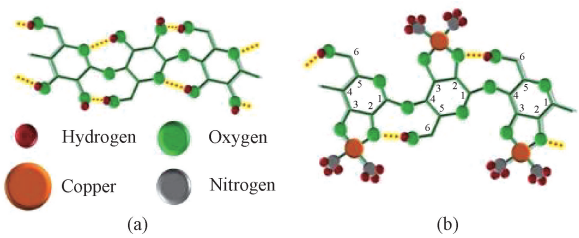

Fig. 1 Schematic diagram of structure: (a) cellulose; (b) cuprammonium cellulose

Electrospinning is a highly adaptable technique that facilitates the formation of nanofibers with regulated morphology, a high volume-to-surface area ratio and customizable mechanical characteristics[18]. Electrospinning can produce nonwoven cellulose membranes for various applications[19-22]. Polyethylene oxide (PEO), a biodegradable polymer soluble in water, has been used for better electrospinnability and mechanical characteristics of the resultant nanofibers. The integration of PEO enhances the intermolecular interaction, resulting in better fiber formation and increased mechanical strength[23]. Moreover, PEO can effectively optimize the fiber diameters and the membrane porosity, enhancing jetting stability during electrospinning and increasing the surface area of the membranes[24].

The main problem with the formation of fibrous materials from electrospinning through pure cellulose solutions is that it frequently results in the production of spherical nanoparticles[25]. Our primary objective is to explore the fabrication process of cellulose-based nanofibers by using cuprammonium solution and investigate their antibacterial properties. We aim to provide a comprehensive understanding of the synthesis methods, characterization techniques, and potential applications of these nanofibers. The combination of cellulose cuprammonium solution with PEO, although intuitively simple, has not been fully elucidated to date, and our study contributes to the existing body of knowledge. We report herein the recent work exploring the binary system based on such combination, demonstrating the benefit in the processing, characteristics and functionality of the nanofibrous membrane system based on cellulose and PEO.

1 Materials and Methods

1.1 Materials

Ammonium hydroxide with a mass fraction range of 28% – 30%, copper (Ⅱ) hydroxide and PEO with relative molecular masses of 300, 500 and 1 000 kDa (denoted as PEO300, PEO500 and PEO1000, respectively) were purchased from Shanghai Aladdin, China. The cotton linter (degree of polymerization of about 1 430) was provided by Central Cotton Research Institute, Multan, Pakistan. The needle wood (degree of polymerization of about 1 185), a softwood pulp of pine tree (pinus), was purchased from Dalian Yangrun, China. Other reagents applied in this research were of analytical quality and obtained from commercial vendors in Qingdao, China. Deionized water was used in the experiments.

1.2 Electrospinning of cellulose nanofibers

Cuprammonium solution with a 2% mass fraction of copper hydroxide was prepared by mixing copper hydroxide with ammonium hydroxide using a magnetic stirrer for 10 min. The cuprammonium solution was utilized to dissolve cellulose. The mass fractions of the cellulose in the solution were maintained at a range of 2% to 5%. The mixture was subjected to magnetic stirring for 30 min. Distinct solutions of PEO with mass fractions ranging from 1.0% to 2.0% were prepared individually and subsequently blended with cellulose solution in varying mass ratios (1∶1, 3∶1 and 4∶1, respectively) of the dissolved cellulose to the PEO solution. Subsequently, following a 15 min mixing period, the compound solution was subjected to electrospinning at ambient temperature. This process was carried out using a needle with an inner diameter of 0.6 mm at supply rates ranging from 1.67 μL/min to 16.67 μL/min and at applied voltages between 15 kV and 27 kV. The distances from the collector were maintained at 100 mm to 160 mm, while the relative humidities (RHs) were kept within a range of 28% to 59%. The obtained nanofibrous

membranes were dried at 60 ℃ for 2 h.

1.3 Characterization

The morphological characteristics of nanofibrous membranes were examined through scanning electron microscopy (SEM) using a Phenom Pro instrument (Hitzacker, Germany). The measurement of fiber diameters was conducted using the NanoMeasurer 1.2.5 software. An electronic extensometer was utilized to analyze the mechanical traits of the nanofibrous membranes. The X-ray diffractometer (XRD) patterns were obtained with a DX-2700 X-ray diffractometer (Japan) with Cu Kα radiation (40 kV, 40 mA), the noted region of 2θ was 5°–80°, and the scanning speed was 5.0 (°)/min. The samples included electrospun nanofibers made from the cotton linter and the needle wood. These nanofibers contained a mass fraction of 3% cellulose and 2% PEO500. X-ray photoelectron spectroscopy (XPS) was employed to examine the bonding states of surface components within the sample. The experiments were conducted using a Thermo Fisher ESCALAB 250Xi spectrometer (Japan) equipped with an Al Kα X-ray source with an energy of 1 486.6 eV.

1.4 Antibacterial activity assessment

The disc diffusion method was used to evaluate the antibacterial effect of nanofibrous membranes against *Staphylococcus aureus* (*S. aureus*) and *Escherichia coli* (*E. coli*)[26]. In a short procedure, the bacterial suspensions (200 μL, 1×10^6 CFU/mL) were introduced onto the solid agar medium and evenly distributed using a glass spreading rod. Initially, the customized samples with a diameter of approximately 16 mm were placed in Petri dishes cultured with *S. aureus* and *E. coli*. Subsequently, the Petri dishes were incubated for 24 h at 37 ℃. The area of inhibition zones surrounding each sample was determined using the ImageJ 1.46r software. The antibacterial tests were conducted in triplicate using samples that were prepared individually.

2 Results and Discussion

2.1 Formation of electrospun nanofibrous membranes

We focused on the interactions between cellulose sources, cellulose mass fractions, PEO mass fractions, PEO relative molecular masses, the cellulose cuprammonium solution's viscosity, and the resultant nanofibers' mean diameter. Table 1 presents the solution compositions of cellulose and PEO, as well as the fiber diameter and morphology. Table 2 displays the pertinent electrospinning process parameters of each sample. No Taylor cone was observed for cellulose cuprammonium solutions within the mass fractions of 1% to 5% at the applied voltage. The electrospinning process resulted in a spherical droplet that increased in size with the increase of cellulose mass fractions. Ultimately, the droplet was sprayed with minimal extension, which deviated from the typical electrospinning process. The solution viscosity played a considerable role in the process of Taylor cone generation and the ability of the polymer solution to generate extended fibers. The escalating mass fractions of cuprammonium cellulose may also induce more pronounced viscoelasticity of the solution which is adverse to the elongational flow, thus impeding the fiber formation. The production of droplets and limited expansion is the result of a decrease in the electric charge, which prevents the formation of a Taylor cone. To tackle this problem and mitigate the internal charges of the solution, PEO has emerged as a promising additive for facilitating the electrospinning process. PEO has a high relative molecular mass and is frequently employed to enhance the spinnability of solutions in electrospinning. It functions to enhance the formation of the Taylor cone due to intermolecular interaction among the hydroxyl groups of cellulose and the ether groups of PEO, thereby assisting in attaining the desired internal charge distribution of the electrospinning process.

Table 1 Cellulose and PEO solution combinations and the fiber properties

Sample	Cellulose source	Cellulose mass fraction in cuprammonium solution/%	PEO relative molecular mass/kDa	PEO mass fraction in aqueous solution/%	Mass ratio of cellulose to PEO in solution	Fiber diameter/nm	Fiber morphology
CL1	Cotton linter	2	300	2.0	1∶1	145±13	Fibers with spindle-like beads
CL2	Cotton linter	3	300	2.0	1∶1	176±24	Fibers with few spindle-like beads
CL3	Cotton linter	4	300	2.0	1∶1	195±13	Beads with few fibers
CL4	Cotton linter	5	300	2.0	1∶1	230±23	Fibers with few beads
CL5	Cotton linter	2	500	2.0	1∶1	130±25	Spindle-like beads with few fibers
CL6	Cotton linter	3	500	2.0	1∶1	215±11	Fibers with spindle-like beads
CL7	Cotton linter	4	500	2.0	1∶1	245±16	Fibers with spindle-like beads
CL8	Cotton linter	5	500	2.0	1∶1	310±23	Few fibers with beads
CL9	Cotton linter	2	1 000	1.0	4∶1	330±17	Fibers with few beads
CL10	Cotton linter	3	1 000	1.5	3∶1	270±24	Fibers with beads

(Table 1 continued)

Sample	Cellulose source	Cellulose mass fraction in cuprammonium solution/%	PEO relative molecular mass/kDa	PEO mass fraction in aqueous solution/%	Mass ratio of cellulose to PEO in solution	Fiber diameter /nm	Fiber morphology
CL11	Cotton linter	4	1 000	1.0	3∶1	—	Electrospraying
NW1	Needle wood	2	300	2.0	1∶1	130±23	Fibers with beads
NW2	Needle wood	3	300	2.0	1∶1	—	Electrospraying
NW3	Needle wood	4	300	2.0	1∶1	—	Electrospraying
NW4	Needle wood	5	300	2.0	1∶1	225±23	Fibers with beads
NW5	Needle wood	2	500	2.0	1∶1	—	Electrospraying
NW6	Needle wood	3	500	2.0	1∶1	—	Electrospraying
NW7	Needle wood	4	500	2.0	1∶1	270±34	Fibers with few beads
NW8	Needle wood	5	500	2.0	1∶1	—	Electrospraying
NW9	Needle wood	2	1 000	1.0	4∶1	310±28	Regular nanofibers
NW10	Needle wood	3	1 000	1.5	3∶1	150±34	Fibers with beads
NW11	Needle wood	4	1 000	1.0	3∶1	350±32	Fibers with spindle-like beads

Table 2 Electrospinning process parameters

Sample	Flow rate/(μL/min)	Applied voltage/kV	Distance/mm	Temperature/℃	RH/%
CL0	6.67	23.05	160	32	39
CL1	6.67	23.05	160	32	39
CL2	6.67	23.07	160	32	38
CL3	5.00	23.11	160	30	42
CL4	8.34	24.63	160	29	43
CL5	8.34	23.05	160	32	39
CL6	8.34	23.05	160	31	39
CL7	8.34	23.07	160	30	41
CL8	8.34	25.10	160	30	42
CL9	8.34	15.81	110	30	30
CL10	16.67	27.24	110	20	31
CL11	7.50	24.00	100	22	44
NW0	5.83	21.78	130	22	44
NW1	5.83	21.78	130	22	44
NW2	5.00	23.05	125	24	38
NW3	6.67	22.85	125	23	30
NW4	2.50	16.00	120	24	42
NW5	3.34	20.48	120	22	44
NW6	5.00	23.12	130	31	40
NW7	5.00	21.11	125	22	36
NW8	1.67	19.12	140	25	43
NW9	8.34	15.80	110	20	28
NW10	11.67	27.22	110	21	39
NW11	16.67	22.10	150	27	48

Previous studies have reported successful electrospinning outcomes with the combined solutions of PEO and other biodegradable polymers[27-29]. However, the mass fractions and molecular masses of PEO and cuprammonium cellulose are different and their effects on spinning and fiber morphology are yet to be explored.

2.2 Characterizations

Figure 2 presents the viscosity of the cotton linter and the needle wood. The viscosity increases with the mass fractions of the cotton linter and the needle wood in the cuprammonium solution. The cotton linter shows high viscosity due to a high degree of polymerization[30-31].

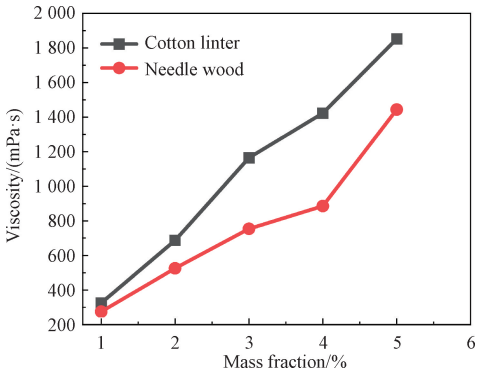

Fig. 2 Viscosity of cotton linter and needle wood in cuprammonium solution

PEO solutions with different relative molecular masses (300, 500 and 1 000 kDa) and different mass fractions (1.0%, 1.5% and 2.0%) are prepared. The obtained solutions are denoted as 2.0%-PEO300, 2.0%-PEO500, 1.0%-PEO1000 and 1.5%-PEO1000, respectively. The nanofibrous membranes obtained from the above solutions are denoted as m-2.0%-PEO300, m-2.0%-PEO500, m-1.0%-PEO1000 and m-1.5%-PEO1000, respectively. Figures 3(a) and 3(b) represent the viscosities of both cellulosic sources in the cuprammonium solution with different mass fractions blended with 2.0%-PEO300. As the mass fraction of cellulose increases, the viscosities of the solution increase. The cotton linter with mass fractions from 2% to 5% in the cuprammonium solution with 2.0%-PEO500 show viscosities of 324, 618, 742 and 957 mPa·s, respectively. The needle wood (Fig. 3(b)) shows relatively lower viscosities than cotton linter and is unable to form jets, which is mainly characterized by the phenomenon of electrospray. As shown in Fig. 3(c), the viscosities of 2%-PEO300, 2%-PEO500, 1%-PEO1000 and 1.5%-PEO1000 are 60.0, 107.1, 176.7 and 245.7 mPa·s, respectively. The viscosities increase with PEO relative molecular masses.

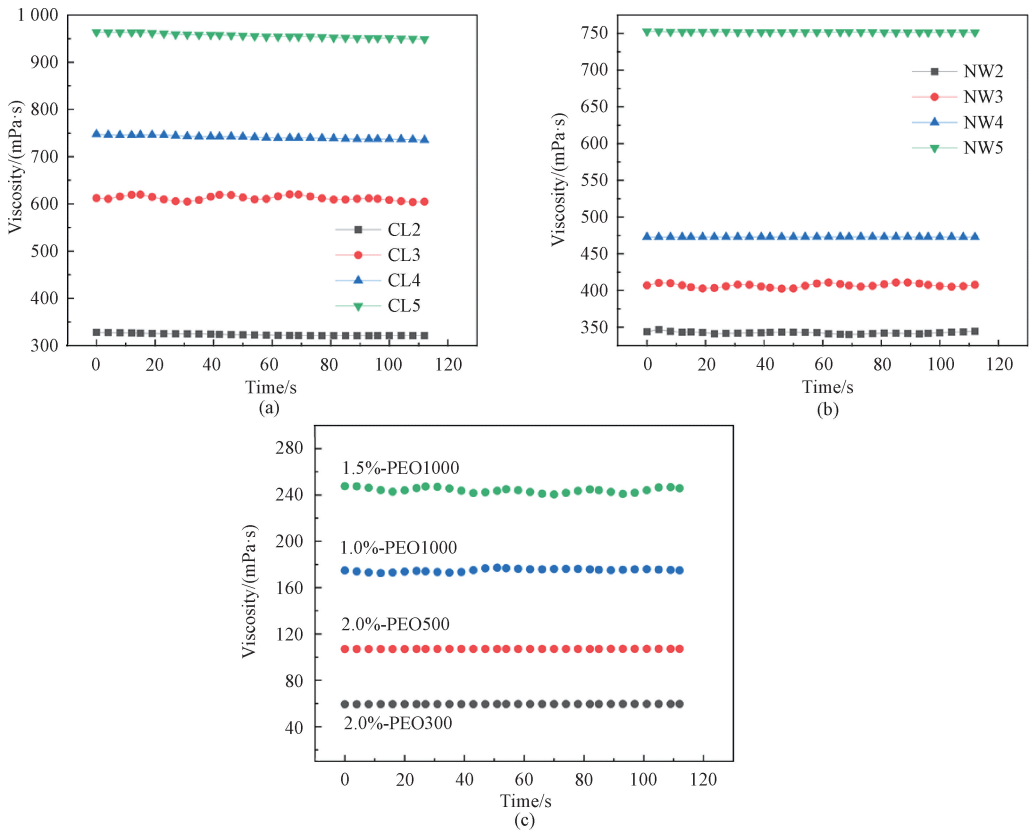

Fig. 3 Viscosities of different samples: (a) cotton linter in cuprammonium solution with 2.0%-PEO300; (b) needle wood in cuprammonium solution with 2.0%-PEO300; (c) PEO solutions with different PEO relative molecular masses and mass fractions

Figure 4 shows the surface morphology of the cotton linter nanofiber samples from CL1 to CL11 (mass fractions ranging from 2% to 5%) with varying relative molecular masses of PEO. Notably, when the cellulose mass fraction exceeds 5%, the electrospinning dispersion is often disrupted by the expulsion of large droplets from the spinneret. The observed phenomenon can be attributed to the solution's elevated viscosity and the cellulose flocculation induced in the dispersion of the separation phases[32].

SEM images of the cotton linter nanofibers (CL2, CL4 and CL9) show a continuous nanofiber with mean diameters of (176±24), (230±23) and (330±17) nm, respectively. Samples CL3 and CL8 show a limited number of nanofibers and beads. Despite attempts to decrease the electric field, the formation of beads remained

inevitable. Noteworthy variations in the diameter and structural morphology of electrospun nanofibers are observed upon varying the relative molecular mass of PEO. Samples CL2 and CL4, which contain cotton linters and PEO300, exhibit uniform nanofibers. In contrast, samples CL5 to CL8, which contain cotton linters and PEO500, display irregular spindle-shaped beads with some fibers. The relative molecular mass of PEO notably influences the spinnability of the solutions. The increase in the bead size and the quantity at a higher PEO relative molecular mass can be attributed to a rise in viscosity and a decrease in the charge density taken by the jet[33]. CL9 shows continuous nanofibers, CL10 has a fibrous and bead-like structure, while CL11 exhibits the electrospraying behavior. The observed phenomenon can be attributed to the lower amount of PEO in CL9. In agreement with the findings of Filip et al.[34], a low amount of PEO with a high relative molecular mass can improve the spinnability of an aqueous sodium alginate solution.

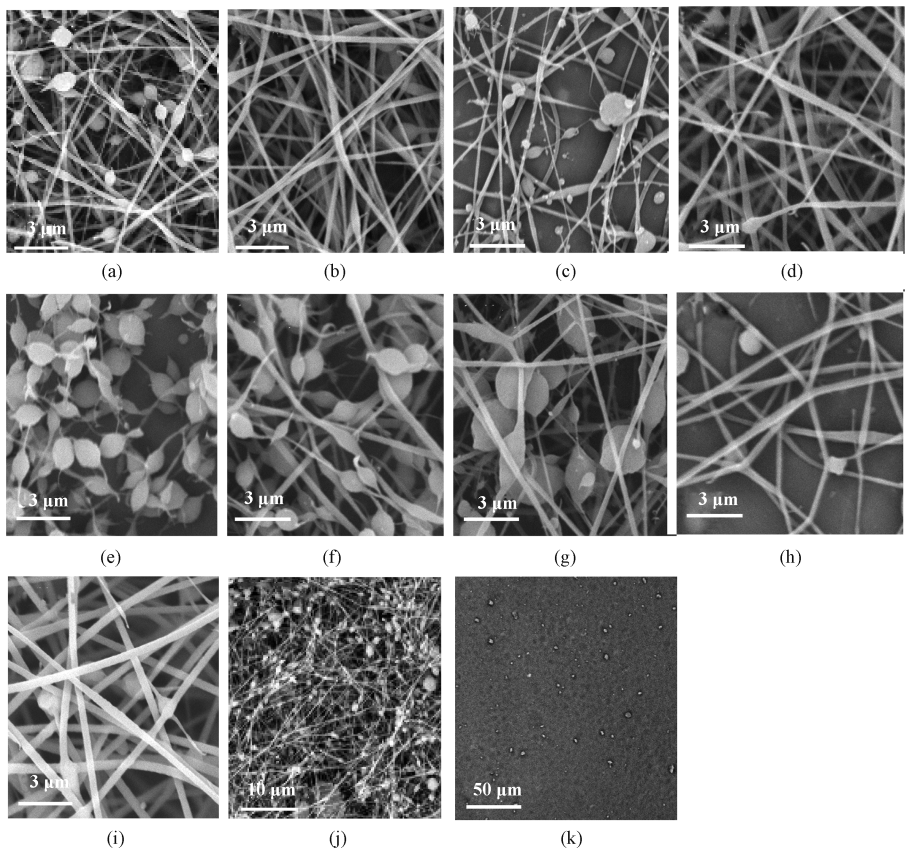

Fig. 4 SEM images of cotton linter nanofiber samples: (a) CL1; (b) CL2; (c) CL3; (d) CL4; (e) CL5; (f) CL6; (g) CL7; (h) CL8; (i) CL9; (j) CL10; (k) CL11

Figure 5 represents the diameter distribution curves depicting the diameter comparison of electrospun fibers from different cellulose mass fractions.

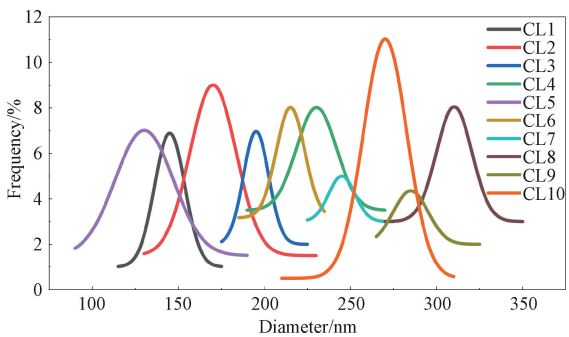

Fig. 5 Diameter distribution curves of samples from CL1 to CL10

The diameters of the fibers with varying cellulose mass fractions and PEO relative molecular masses fall in a range of 100 nm to 350 nm. Samples CL1 to CL4 have fiber diameters ranging from (145 ± 13) nm to (230 ± 23) nm. The increase in the fiber diameter in response to the elevated mass fractions of cotton linters is attributed to the higher cellulose mass fraction and the increased viscosity[35-36].

Figure 6 illustrates the surface morphology of the needle wood nanofiber samples from NW1 to NW11 which are prepared using needle wood and PEO. SEM images of the needle wood nanofibers (NW1, NW7 and NW11) show continuous nanofibers with mean diameters of (130 ± 23), (270 ± 34) and (310 ± 28) nm, respectively. The electrospinnability behavior of the

needle wood cellulose exhibited dissimilarities compared to that of the cotton linter. Most of the compositions exhibit electrospraying rather than electrospinning. Regular nanofibers are observed solely in samples NW1, NW7 and NW11. The lower viscosity of the needle wood in the cuprammonium solution as compared to the cotton linter is the reason for this phenomenon. A solution characterized by low viscosity exhibits a correspondingly low viscoelastic force, rendering it insufficient to counterbalance the electrostatic repulsion forces that act upon the stretching of the electrospinning jet. This phenomenon results in the partial fragmentation of the jet[37]. Figure 7 displays the diameter distribution curves of needle wood nanofibers generated from diverse PEO relative molecular masses at various needle wood mass fractions. The diameters of needle wood nanofibers fall in 100–382 nm.

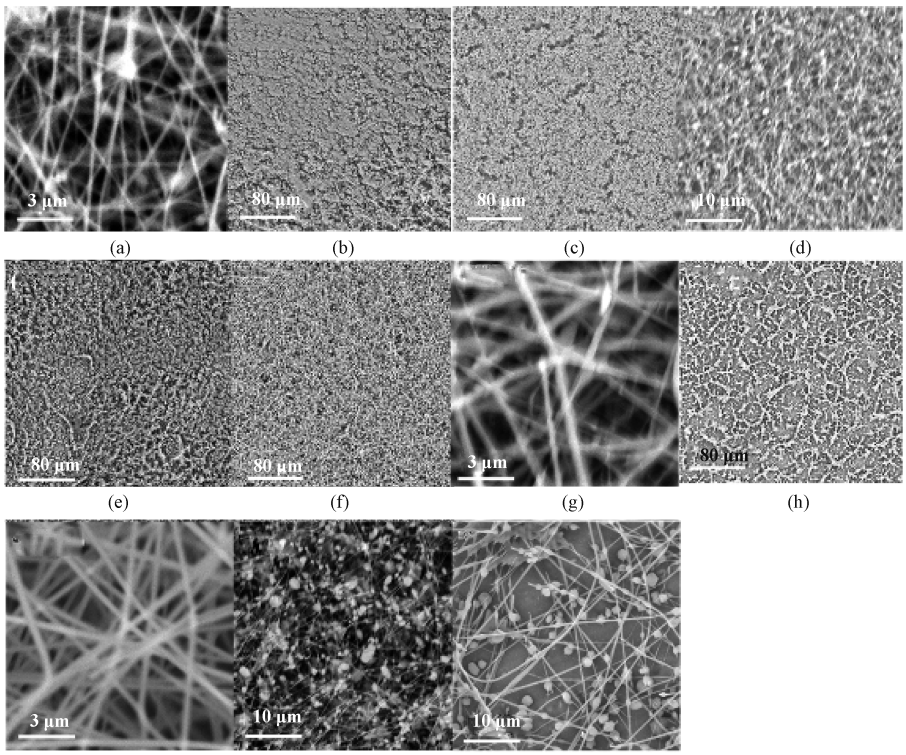

Fig. 6 SEM images of needle wood nanofiber samples: (a) NW1; (b) NW2; (c) NW3; (d) NW4; (e) NW5; (f) NW6; (g) NW7; (h) NW8; (i) NW9; (j) NW10; (k) NW11

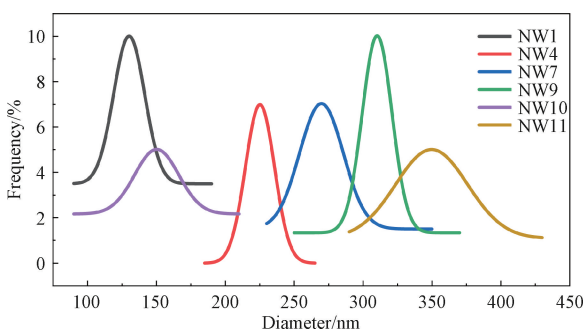

Fig. 7 Diameter distribution curves of samples NW1, NW4, NW7, NW9 to NW11

Tensile strengths and elongations at break of nanofibrous membranes are shown in Fig. 8. The tensile strengths of the samples from CL1 to CL9 are 3.23, 3.54, 3.85, 4.28, 3.55, 4.32, 4.51, 4.55 and 5.23 MPa, respectively, whereas the tensile strengths of NW1, NW7, NW9 and NW11 are 2.99, 4.27, 4.82, and 5.02 MPa, respectively. The elongations at break of the samples from CL1 to CL9 are 20.33%, 21.58%, 23.81%, 25.62%, 25.53%, 26.2%, 28.2%, 31.29% and 41.4%, respectively, whereas the elongation at break of NW1, NW7, NW9 and NW11 are 19.45%, 25.56%, 37.8% and 39.53%, respectively. The tensile strength increases with an increase in the cellulose mass fraction and the PEO relative molecular mass for both cellulosic sources, and the elongation at break shows the same trend. It can be seen that CL9 and NW9 show increased elongation at break compared to other samples. Tensile strengths and elongations at break of pure PEO with different relative molecular masses are shown in Fig. 8(c). The tensile strengths and the elongations at break for m-2.0%-PEO300, m-2.0%-PEO500 and m-1.0%-PEO1000 are 1.67, 2.37 and 3.91 MPa, and 8.25%, 14.19% and 30.92%, respectively. Pure PEO

shows low strength and elongation at break as compared to that blended with cellulose.

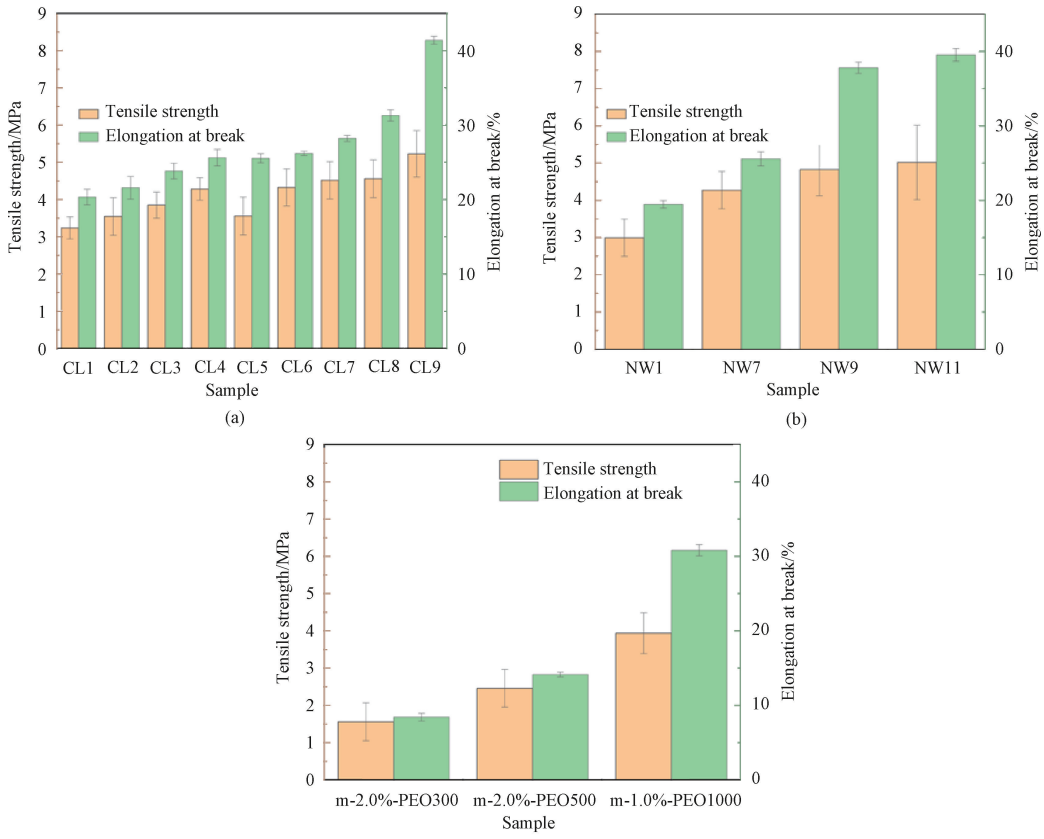

Fig. 8 Comparison of tensile properties of various nanofibrous membranes: (a) cotton linter/PEO; (b) needle wood/PEO; (c) PEO with different relative molecular masses and mass fractions

XRD is utilized to analyze the original materials and the structural disparities in the electrospun material (Fig. 9). The utilization of liquid ammonia for cellulose treatment facilitates the processing of cellulose fibers reacting with hydroxyl groups, subsequently disrupting hydrogen bonds, and thereby accelerating the swelling of cellulose fibers[38-39].

The crystallinity X_c is determined using XRD and calculated as[39]

$$X_c = \left(\frac{A_c}{A_c + A_a}\right) \times 100\%,$$

where A_c and A_a are the area of crystalline and amorphous regions, respectively.

Figures 9(a) and 9(b) indicate the diffraction peaks of the cotton linter and the needle wood at 2θ around 15.8°, 22.9°, 34.5°, and 15.7°, 22.8°, 34.9°, respectively. The peaks are attributed to the planes of (101), (002) and (040), which are in agreement with the characteristic diffraction peaks of cellulose I[40-42]. The XRD patterns of the cotton linter and the needle wood nanofibrous membrane, shown in Figs. 9(c) and 9(d), display prominent peaks at 19.2° and 19.1°, respectively. These peaks suggest the presence of PEO[43]. The distinct peaks at approximately 21.7° for the cotton linter, and 11.4°, 21.3° and 37.0° for the needle wood are the evidence of cellulose Ⅲ[22,44]. The transition from cellulose Ⅰ to cellulose Ⅲ can be detected by monitoring the displacement of the (002) peak, which undergoes a shift in its 2θ value from 22.8° to 21.3° during the conversion process[39]. The crystallinity of cuprammonium cotton linter and needle wood is 54.6% and 54.2%, respectively. Dissolution of cellulose in cuprammonium induces disruption of the long-range crystalline arrangement, leading to lower crystallinity.

The XPS spectra of cuprammonium cellulose/PEO nanofibrous membrane are given in Fig. 10. In a theoretical context, it has been observed that pure cellulose demonstrates two distinct peaks of carbon and oxygen in the full XPS spectra[45-46]. The XPS spectra of cellulose/PEO nanofiber displayed three signals at around 284 eV and 531 eV for carbon and oxygen, and 931 eV which was associated with the presence of copper atoms[47].

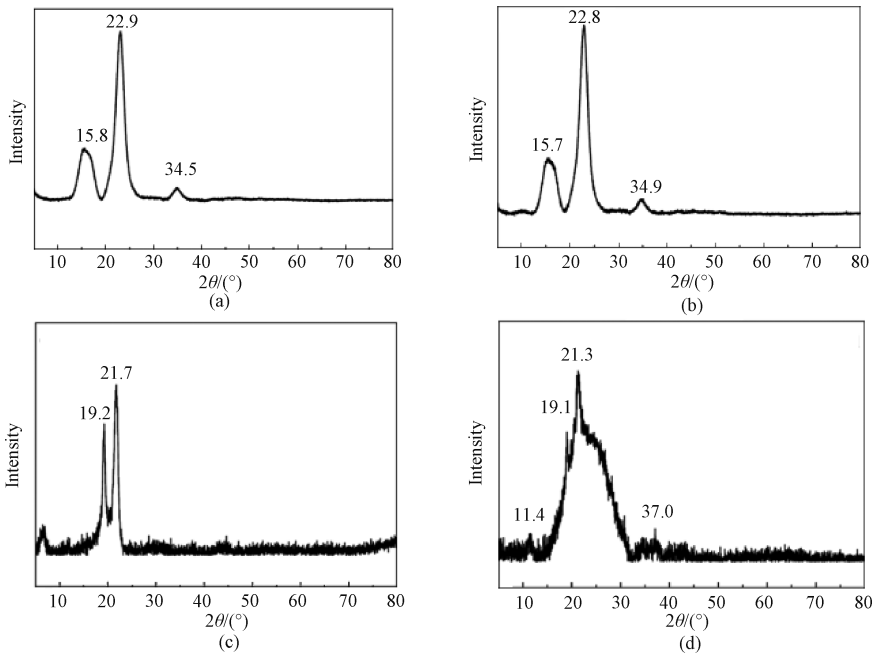

Fig. 9 XRD patterns: (a) cotton linter; (b) needle wood; (c) electrospun cotton linter nanofibrous membrane; (d) electrospun needle wood nanofibrous membrane

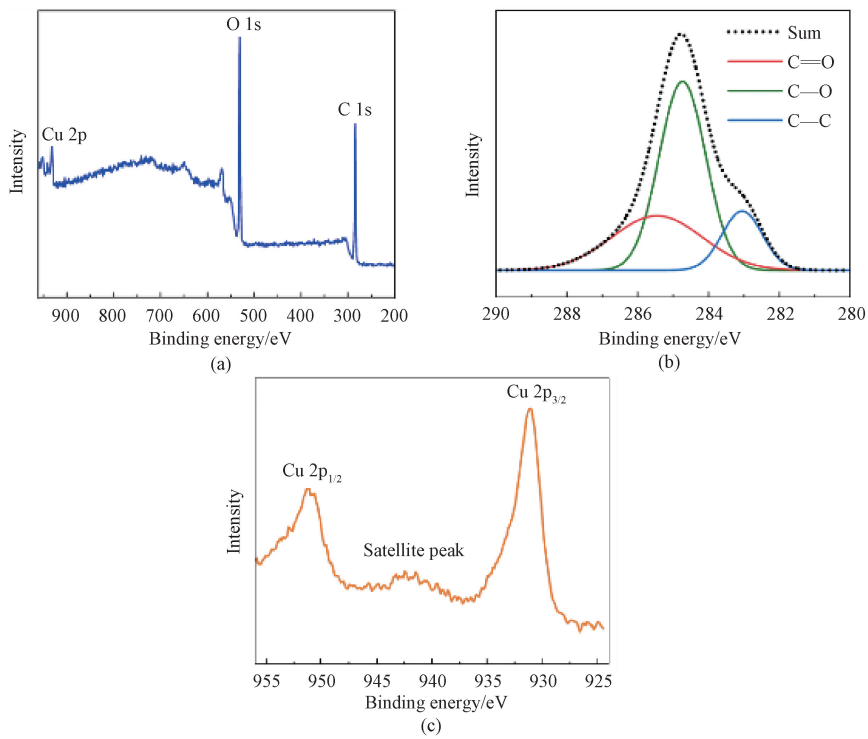

Fig. 10 XPS spectra of cuprammonium cellulose/PEO nanofibrous membrane: (a) full spectrum; (b) C 1s spectra; (c) main and satellite peaks of Cu 2p

The high-resolution XPS spectrum of C 1s of cuprammonium cellulose/PEO nanofibrous membrane shows C—C, C—O and C═O groups (Fig. 10(b)). The C—C connections often involve the carbon atoms primarily derived from cellulose[48-49]. The carbon atoms connect non-carbonyl oxygen atoms to form C—OH, in which the oxygen atoms are primarily derived from cellulose[48,50]. The C 1s peak appears when the carbon atom is bonded to either two non-carbonyl oxygen atoms (O—C—O) or a single carbonyl oxygen atom (C═O)[51]. The binding energy associated with the O 1s orbital engaged in the —C═O moiety is estimated to be

approximately 531.4 eV[52]. Figure 10(c) shows XPS peaks around 931 eV and 951 eV characteristic for Cu $2p_{3/2}$ and Cu $2p_{1/2}$, respectively. The characteristic $2p_{3/2}$ binding energy at 931 eV, separating from $2p_{1/2}$ by 20 eV[53-54], indicates the presence of Cu^{2+}.

2.3 Antibacterial activity

The disc diffusion method was used to examine the antibacterial properties of nanofibrous membranes. The quantification of the growth of bacteria on the agar plates was determined by measuring the area of the inhibition zone(Fig. 11).

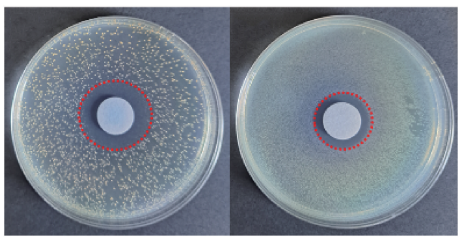

(a) (b)

Fig. 11 Images of bacterial survival on agar plates following contact with nanofibrous membrane: (a) *S. aureus*; (b) *E. coli*

The area of the inhibition zone of *S. aureus* and *E. coli* are (15.10 ± 0.71) mm^2 and (8.04 ± 0.24) mm^2, respectively. The red circles signify the effectiveness of membranes against bacterial clones. The findings of this study show that the electrospun membranes exhibit exceptional antibacterial properties. There is a possibility that copper ions are released into the surrounding environment, leading to the manifestation of strong bactericidal properties[55]. The presence of amine and carboxyl groups on the cell surface of bacteria makes the liberated Cu^{2+} extremely attractive to them. Cell membrane disruption may occur as a result of this attraction, resulting in impaired enzyme performance or damage to crucial biochemical processes. In addition, Cu^{2+} can traverse the cell membrane and potentially impact the functionality of biomolecules[56]. As a result of double bond oxidation in phospholipids, oxidative stress can occur and bacterial cell development can be hindered. Consequently, membrane fluidity can be enhanced[57] or proteins responsible for bonding and biofilm formation may be disrupted[58].

3 Conclusions

This study presented a successful aqueous binary system formulation enabling the electrospinning of cellulose-based nanofibers. This formulation allowed the production of functionalized nanofibrous membranes through a streamlined spinning process bypassing the need for a complex and environmentally burdensome combination of exotic organic solvents, presenting a more sustainable alternative. In the cuprammonium cellulose solution, high relative molecular mass PEO at low mass fractions and low relative molecular mass PEO were both effective in producing smooth nanofibers. These nanofibers exhibited diameters within the range of 130 nm to 382 nm. The fiber diameter increased with the increase of the cellulose mass fraction and the PEO relative molecular mass. The needle wood exhibited poorer spinnability than the cotton linter. The conversion of the crystalline structure cellulose I to cellulose Ⅲ occured during the nanofiber formation due to the dissolution-spinning-recovery process in the cuprammonium solution. The nanofibrous membrane also showed antibacterial activity against *S. aureus* and *E. coli* owing to copper ions on the membrane surface, as indicated by XPS analyses. As a result of high surface area, controllable cellulose structure and antibacterial efficacy, cuprammonium cellulose/PEO nanofibrous membranes can potentially be used in water treatment, energy storage and food packaging.

References

[1] HABIBI Y. Key advances in the chemical modification of nanocelluloses[J]. *Chemical Society Reviews*, 2014, 43(5): 1519-1542.

[2] DAHIYA A. Cellulosic fibers and nonwovens from solutions: processing and properties[D]. Knoxville: The University of Tennessee, 2006.

[3] RAZALI R A, LOKANATHAN Y, CHOWDHURY S R, et al. Physicochemical and structural characterization of surface modified electrospun PMMA nanofibre[J]. *Sains Malaysiana*, 2018, 47(8): 1787-1794.

[4] KUMI A K, FAN R L, ZHANG Y, et al. Preparation and properties of regenerated cellulose/amylopectin blend fibers from 1-butyl-3-methylimidazolium chloride with controlled biodegradation[J]. *Journal of Donghua University (English Edition)*. 2024, 41(5): 461-473.

[5] ROJAS O J. Cellulose chemistry and properties: fibers, nanocelluloses and advanced materials[M]. Cham: Springer, 2016.

[6] SZABÓ L, MILOTSKYI R, SHARMA G, et al. Cellulose processing in ionic liquids from a materials science perspective: turning a versatile biopolymer into the cornerstone of our sustainable future[J]. *Green Chemistry*, 2023, 25(14): 5338-5389.

[7] HACHAICHI A, KOUINI B, KIAN L K, et al. Nanocrystalline cellulose from microcrystalline cellulose of date palm fibers as a promising candidate for bio-nanocomposites: isolation and characterization[J]. *Materials*, 2021, 14(18): 5313.

[8] ELSEOUD O A, KOSTAG M, JEDVERT K, et al. Cellulose in ionic liquids and alkaline solutions: advances in the mechanisms of

biopolymer dissolution and regeneration [J]. *Polymers*, 2019, 11(12): 1917.
[9] COSTA C, MEDRONHO B, FILIPE A, et al. Emulsion formation and stabilization by biomolecules: the leading role of cellulose [J]. *Polymers*, 2019, 11(10): 1570.
[10] ZHU B J, LI Z, CHEN S Y, et al. Bacterial cellulose nanofibers as reinforcement for preparation of bamboo pulp-based composite paper [J]. *Journal of Donghua University (English Edition)*, 2023, 40(3): 247-254.
[11] SAYYED A J, DESHMUKH N A, PINJARI D V. A critical review of manufacturing processes used in regenerated cellulosic fibers: viscose, cellulose acetate, cuprammonium, LiCl/DMAc, ionic liquids, and NMMO based Lyocell [J]. *Cellulose*, 2019, 26(5): 2913-2940.
[12] DIAS Y J, KOLBASOV A, SINHA-RAY S, et al. Theoretical and experimental study of dissolution mechanism of cellulose [J]. *Journal of Molecular Liquids*, 2020, 312: 113450.
[13] SAALWÄCHTER K, BURCHARD W, KLÜFERS P, et al. Cellulose solutions in water containing metal complexes [J]. *Macromolecules*, 2000, 33(11): 4094-4107.
[14] REEVES R E. Cuprammonium-glycoside complexes [J]. *Advances in Carbohydrate Chemistry*, 1951, 6: 107-134.
[15] SAALWÄCHTER K, BURCHARD W. Cellulose in new metal-complexing solvents. 2. semidilute behavior in Cd-tren [J]. *Macromolecules*, 2001, 34(16): 5587-5598.
[16] MIYAMOTO I, MATSUOKA Y, MATSUI T, et al. Studies on structure of cuprammonium cellulose Ⅲ. structure of regenerated cellulose treated by cuprammonium solution [J]. *Polymer Journal*, 1996, 28(3): 276-281.
[17] ZHANG Z Y, WEI J Y, ZHANG X L, et al. Polyester fabrics coated with cupric hydroxide and cellulose for the treatment of kitchen oily wastewater [J]. *Chemosphere*, 2022, 302: 134840.
[18] ADAMU B F, GAO J, JHATIAL A K, et al. A review of medicinal plant-based bioactive electrospun nano fibrous wound dressings [J]. *Materials & Design*, 2021, 209: 109942.
[19] TEIXEIRA M A, PAIVA M C, et al. Electrospun nanocomposites containing cellulose and its derivatives modified with specialized biomolecules for an enhanced wound healing [J]. *Nanomaterials*, 2020, 10(3): 557.
[20] GE L, YIN J J, YAN D W, et al. Construction of nanocrystalline cellulose-based composite fiber films with excellent porosity performances via an electrospinning strategy [J]. *ACS Omega*, 2021, 6(7): 4958-4967.
[21] LI C H, MU J H, SONG Y J, et al. Highly aligned cellulose/polypyrrole composite nanofibers via electrospinning and in situ polymerization for anisotropic flexible strain sensor [J]. *ACS Applied Materials & Interfaces*, 2023: 15(7): 9820-9829.
[22] DIZGE N, SHAULSKY E, KARANIKOLA V. Electrospun cellulose nanofibers for superhydrophobic and oleophobic membranes [J]. *Journal of Membrane Science*, 2019, 590: 117271.
[23] ZAITOON A, LIM L T. Effect of poly(ethylene oxide) on the electrospinning behavior and characteristics of ethyl cellulose composite fibers [J]. *Materialia*, 2020, 10: 100649.
[24] FAWAL E, FAROUK G. Polymer nanofibers electrospinning: a review [J]. *Egyptian Journal of Chemistry*, 2020, 63(4): 1279-1303.
[25] QI H S, SUI X F, YUAN J Y, et al. Electrospinning of cellulose-based fibers from NaOH/urea aqueous system [J]. *Macromolecular Materials and Engineering*, 2010, 295(8): 695-700.
[26] LIU S P, LI J W, ZHANG S H, et al. Template-assisted magnetron sputtering of cotton nonwovens for wound healing application [J]. *ACS Applied Bio Materials*, 2020, 3(2): 848-858.
[27] GAO J, GUO H W, ZHAO L S, et al. Water-stability and biological behavior of electrospun collagen/PEO fibers by environmental friendly crosslinking [J]. *Fibers and Polymers*, 2017, 18(8): 1496-1503.
[28] NIKBAKHT M, SALEHI M, REZAYAT S M, et al. Various parameters in the preparation of chitosan/polyethylene oxide electrospun nanofibers containing Aloe vera extract for medical applications [J]. *Nanomedicine Journal*, 2020, 7(1): 21-28.
[29] CHEN G K, GUO J X, NIE J, et al. Preparation, characterization, and application of PEO/HA core shell nanofibers based on electric field induced phase separation during electrospinning [J]. *Polymer*, 2016, 83: 12-19.
[30] MONSHIZADEH A. Influence of the molecular weight of cellulose on the solubility in ionic liquid-water mixtures [D]. Helsinki: Aalto University, 2015.
[31] HALLAC B B, RAGAUSKAS A J. Analyzing cellulose degree of polymerization and its relevancy to cellulosic ethanol [J]. *Biofuels, Bioproducts and Biorefining*, 2011, 5(2): 215-225.
[32] OLSSON R T, KRAEMER R, LÓPEZ-RUBIO A, et al. Extraction of microfibrils from bacterial cellulose networks for electrospinning of anisotropic biohybrid fiber yarns [J]. *Macromolecules*, 2010, 43(9): 4201-4209.

[33] DESHAWAR D, GUPTA K, CHOKSHI P. Electrospinning of polymer solutions: an analysis of instability in a thinning jet with solvent evaporation[J]. *Polymer*, 2020, 202: 122656.
[34] FILIP P, PEER P. Characterization of poly (ethylene oxide) nanofibers: mutual relations between mean diameter of electrospun nanofibers and solution characteristics[J]. *Processes*, 2019, 7(12): 948.
[35] GULZAR S, TAGRIDA M, NILSUWAN K, et al. Electrospinning of gelatin/chitosan nanofibers incorporated with tannic acid and chitooligosaccharides on polylactic acid film: characteristics and bioactivities [J]. *Food Hydrocolloids*, 2022, 133: 107916.
[36] ANGEL N, LI S N, YAN F, et al. Recent advances in electrospinning of nanofibers from bio-based carbohydrate polymers and their applications [J]. *Trends in Food Science & Technology*, 2022, 120: 308-324.
[37] MIT-UPPATHAM C, NITHITANAKUL M, SUPAPHOL P. Ultrafine electrospun polyamide-6 fibers: effect of solution conditions on morphology and average fiber diameter [J]. *Macromolecular Chemistry and Physics*, 2004, 205(17): 2327-2338.
[38] WADA M, NISHIYAMA Y, LANGAN P. X-ray structure of ammonia-cellulose I: new insights into the conversion of cellulose I to cellulose III_I [J]. *Macromolecules*, 2006, 39 (8): 2947-2952.
[39] MITTAL A, KATAHIRA R, HIMMEL M E, et al. Effects of alkaline or liquid-ammonia treatment on crystalline cellulose: changes in crystalline structure and effects on enzymatic digestibility [J]. *Biotechnology for Biofuels*, 2011, 4: 41.
[40] ZHAO R H, CAI S Z, ZHAO Y T, et al. Enhanced stereo complex crystalline polylactic acids in melt processed enantiomeric bicomponent fiber configurations[J]. *International Journal of Biological Macromolecules*, 2023, 253 (5): 127123.
[41] FRENCH A D. Idealized powder diffraction patterns for cellulose polymorphs[J]. *Cellulose*, 2014, 21(2): 885-896.
[42] WONG S S, KASAPIS S, TAN Y M. Bacterial and plant cellulose modification using ultrasound irradiation[J]. *Carbohydrate Polymers*, 2009, 77(2): 280-287.
[43] YANG S Y, LIU Z M, LIU Y P, et al. Effect of molecular weight on conformational changes of PEO: an infrared spectroscopic analysis [J]. *Journal of Materials Science*, 2015, 50 (4): 1544-1552.
[44] ABOU-SEKKINA M M, SAKRAN M A, SAAFAN A A. Development of correlations among the spectral, structural, and electrical properties and chemical treatment of Egyptian cotton fabric strips[J]. *Industrial & Engineering Chemistry Product Research and Development*, 1986, 25(4): 676-680.
[45] BELGACEM M N, CZEREMUSZKIN G, SAPIEHA S, et al. Surface characterization of cellulose fibers by XPS and inverse gas chromatography [J]. *Cellulose*, 1995, 2 (3): 145-157.
[46] JOHANSSON L S, CAMPBELL J M, ROJAS O J. Cellulose as the in situ reference for organic XPS. Why? Because it works[J]. *Surface and Interface Analysis*, 2020, 52(12): 1134-1138.
[47] MONGIOVÍ C, CRINI G, GABRION X, et al. Revealing the adsorption mechanism of copper on hemp-based materials through EDX, nano-CT, XPS, FTIR, Raman, and XANES characterization techniques [J]. *Chemical Engineering Journal Advances*, 2022, 10: 100282.
[48] KAMDEM D P, RIEDL B, ADNOT A, et al. ESCA spectroscopy of poly (methyl methacrylate) grafted onto wood fibers [J]. *Journal of Applied Polymer Science*, 1991, 43 (10): 1901-1912.
[49] JOHANSSON L S, CAMPBELL J M. Reproducible XPS on biopolymers: cellulose studies [J]. *Surface and Interface Analysis*, 2004, 36(8): 1018-1022.
[50] JOHANSSON L S, CAMPBELL J M, HÄNNINEN T, et al. XPS and the medium-dependent surface adaptation of cellulose in wood [J]. *Surface and Interface Analysis*, 2012, 44 (8): 899-903.
[51] STARK N M, MATUANA L M. Surface chemistry changes of weathered HDPE/wood-flour composites studied by XPS and FTIR spectroscopy [J]. *Polymer Degradation and Stability*, 2004, 86(1): 1-9.
[52] NZOKOU P, PASCAL KAMDEM D. X-ray photoelectron spectroscopy study of red oak-(*Quercus rubra*), black cherry-(*Prunus serotina*) and red pine-(*Pinus resinosa*) extracted wood surfaces [J]. *Surface and Interface Analysis*, 2005, 37(8): 689-694.
[53] MAO P, QI L Y, LIU X D, et al. Synthesis of Cu/Cu_2O hydrides for enhanced removal of iodide from water [J]. *Journal of Hazardous Materials*, 2017, 328: 21-28.
[54] JIANG X, YING D W, LIU X, et al. Identification of the role of Cu site in Ni-Cu hydroxide for robust and high selective electrochemical ammonia oxidation to nitrite[J]. *Electrochimica Acta*, 2020, 345: 136157.
[55] KAUL L, ABDO A I, COENYE T, et al. The combination of diethyldithiocarbamate and copper ions is active against *Staphylococcus aureus* and

Staphylococcus epidermidis biofilms in vitro and in vivo[J]. *Frontiers in Microbiology*, 2022, 13: 999893.

[56] KHANDELWAL M, KUMAWAT A, MISRA K P, et al. Efficient antibacterial activity in copper oxide nanoparticles biosynthesized via *Jasminum sambac* flower extract[J]. *Particulate Science and Technology*, 2023, 41(5): 640-652.

[57] KHASHAN K S, SULAIMAN G M, ABDULAMEER F A. Synthesis and antibacterial activity of CuO nanoparticles suspension induced by laser ablation in liquid[J]. *Arabian Journal for Science and Engineering*, 2016, 41(1): 301-310.

[58] XING C L, CHANG J N, MA M, et al. Ultrahigh-efficiency antibacterial and adsorption performance induced by copper-substituted polyoxomolybdate-decorated graphene oxide nanocomposites[J]. *Journal of Colloid and Interface Science*, 2022, 612: 664-678.

铜氨溶液静电纺丝纤维素基纳米纤维:制备、力学性能和抗菌性

DANISH Iqbal[1,2,3], 赵壬海[1,2], MUHAMMAD Ilyas Sarwar[3], 宁 新[1,2*]

1. 青岛大学 纺织服装学院, 非织造材料与产业用纺织品创新研究院, 山东 青岛 266071, 中国

2. 青岛大学, 山东省特型非织造材料工程研究中心, 山东 青岛 266071, 中国

3. 棉花研究所纤维技术部, 木尔坦 60000, 巴基斯坦

摘 要: 纤维素基纳米纤维因其优异的生物相容性和物理化学特性而备受关注, 并被广泛应用。该研究介绍了一种简单易行的静电纺丝工艺及用其制得的纤维素基纳米材料。采用经典的纤维素-铜氨溶液, 从而避免使用更复杂的化学溶剂组合。进一步将聚环氧乙烷(polyethylene oxide, PEO)引入二元聚合物体系, 改善了静电纺丝过程的稳定性及最终材料的性能, 此过程不涉及有机溶剂。研究了纤维素来源和质量分数及 PEO 配方对纺丝性能和纤维形貌的影响, 并使用铜氨溶液成功制备了直径为 130~382 nm 的纤维。X 射线光电子能谱(X-ray photoelectron spectroscopy, XPS)分析证实了纳米纤维中铜的存在。铜氨溶液对纳米纤维形态内部由纤维素 I 向纤维素 III 晶体结构的转变存在显著影响。同时, 纳米纤维膜表现出对金黄色葡萄球菌和大肠杆菌优异的抗菌性。

关键词: 纤维素; 静电纺丝; 铜氨溶液; 聚环氧乙烷(PEO); 抗菌性